A Dual-Band Metamaterial Antenna

by

Reza Ashtari

A thesis submitted to the Graduate Faculty of
Auburn University
in partial fulfillment of the
requirements for the Degree of
Master of Science in Electrical Engineering

Auburn, Alabama
May 4, 2014

Keywords: Metamaterial, Split Ring Resonator, Dual-band, Antenna

Approved by

Dr. Lloyd Riggs, Professor of Electrical and Computer Engineering
Dr. Michael Baginski, Associate Professor of Electrical and Computer Engineering
Dr. Shiwen Mao, Associate Professor of Electrical and Computer Engineering

Abstract

Metamaterials have a wide variety of potential applications in areas such as optics, acoustics and RF design. Split-Ring Resonators (SRR) are fundamental sub-wavelength structures found in metamaterial design. An adaptation of these SRR's known as Anisotropic Ring Resonators (ARR) is used in this application. When used in antenna design, these sub-wavelength metamaterial structures may exhibit features not found among conventional antenna geometries. Through the combination of various forms of these structures, different applications such as wide-banding, gain maximization and anti-radar performance can be achieved.

An in depth investigation was performed on a metamaterial disc antenna design to examine the potential benefits of these sub-wavelength components in the wide-banding of patch antennas (a.k.a. planar antennas). Several methods in antenna wide-banding such as the use of thicker substrates and edge-coupled patches are employed in conjunction with the ARR and monopole disc antenna to increase the effective reception frequency range from 6.3 GHz to nearly 9.4 GHz through dual band performance.

The two-dimensional antenna is simulated on an FR-4 substrate and has a single side of copper cladding 18um thick (1/2 oz.). Modeling and simulation of the antenna were performed using finite-element method in High Frequency Structure Simulator (HFSS) and Agilent Advanced Design System (ADS).

Acknowledgements

The author would like to thank the following:

- His advisor, Dr. Lloyd Riggs for guidance
- His committee members Dr. Michael Baginski and Dr. Shiwen Mao
- Dr. Michael Hamilton for use of facilities and supplies
- Mr. Joe Haggerty for fabrication assistance
- ANSYS High Frequency Structural Simulator and Agilent Advanced Designed System

Table of Contents

List of Figures

List of Tables

1. Introduction

Metamaterials are artificial structures sized smaller than the wavelength of external stimuli which may exhibit properties not otherwise found in nature. These structures may be made of conventional PC board material such as copper and FR-4. Metamaterial structures rely heavily on their geometry, size, periodicity, alignment and several other factors in order to exhibit behavior such as backward wave propagation or effectively “cloaking”.

Within antenna design, metamaterials are now being used to create “superlenses” that when used with an appropriate antenna, exhibit spatial resolution below that of the wavelength presumed. In addition to the improved resolution and gain in radar applications, an emerging application of these technologies is in discretized battlefield communications. It is a necessity to reduce unwanted radiation in battlefield environments and reduce the possibility of detection. Metamaterial antennas provide a foundation for such a discrete means of communication. Like any antenna, radiation is required to transmit information. However, during information reception it is theorized the use of metamaterial antennas greatly mitigates antenna re-radiation.

With the addition of a metamaterial element and several wide-banding techniques, the antenna's effective frequency reception (-10dB) is measured to resonate at two bands ranging from 6.3 GHz to 7.5 GHz and 8.4 GHz to 9.5 GHz.

2. Literature Review

In this chapter, various patch antennas, substrates, wide-banding techniques and split-ring resonators will be discussed. The antenna studied in this work is a conglomerate of several fundamental planar antenna elements. The foundation upon which everything is built is the disc antenna, which is surrounded by a metamaterial ring resonator. The feeds to the disc and ring elements are tapered accordingly and along the feed have two parasitic components intended for both impedance matching and wide-banding.

2.1. Patch Antennas

Planar or "patch" antennas are two-dimensional antennas and are the standard in today's packaged communications due to their reduced area and volume. The antenna is comprised of one or more conductive layers and one or more substrates. The conventional patch antenna consisting of a single layer of substrate is either microstrip,

coplanar-waveguide (CPW), or stripline. For the antenna design analyzed in this experiment, single-sided CPW was used.

2.1.1. Disc Antenna

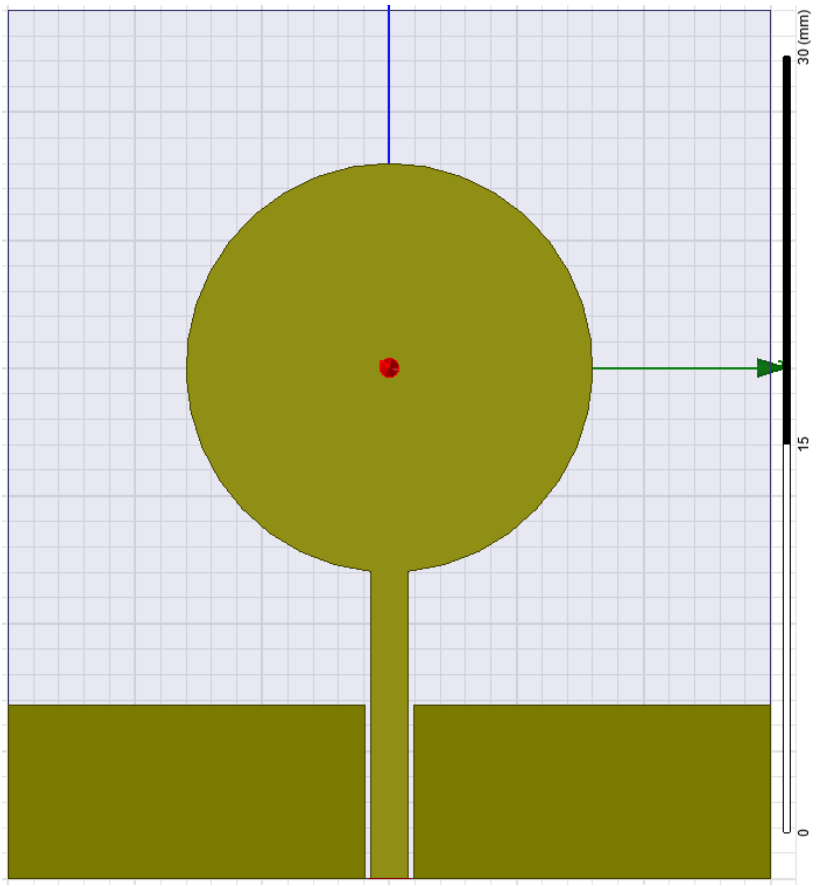

Figure 2.1.1 – Disc Antenna

Disc antennas such as shown in figure 2.1.1 are one of the primary antenna geometries used in patch antenna design. The disc antenna typically radiates a strong and isolated narrowband signal around its intended frequency. Adding the two rectangular parasitic edge-coupled patches to the monopole disc partially alleviates this stronger

single band and uses that energy towards exciting the two lower frequency resonances associated with the height and width of the rectangular patches.

2.1.2. Anisotropic Ring Resonator (ARR) Antenna

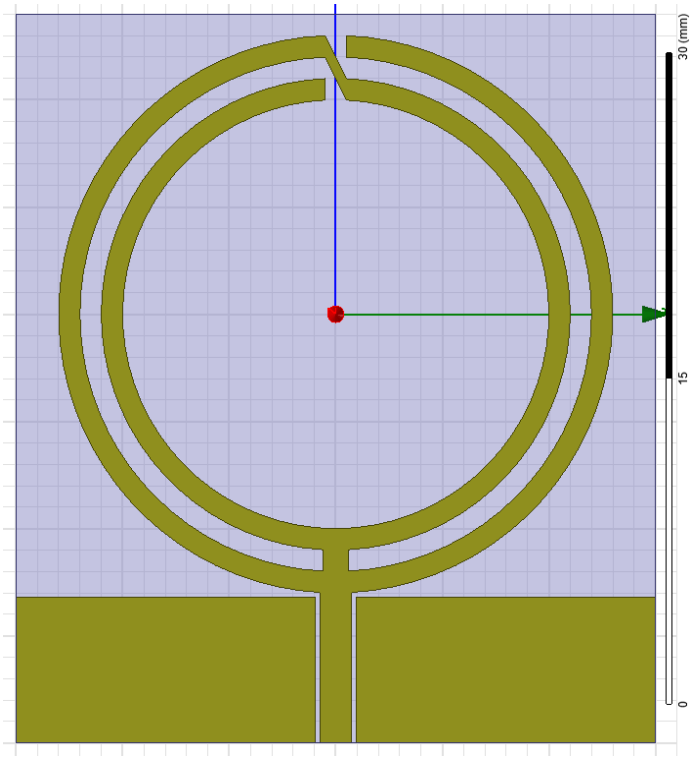

Figure 2.1.2 – ARR Antenna

The anisotropic ring resonator antenna depicted in figure 2.1.2 uses a feed similar to that of the disc antenna, however due to the added ring elements, the impedance of the structure needs to be compensated for accordingly. In addition to the edge coupled patches, to match the impedance of the ARR antenna, a logarithmic taper was introduced into the feed. As each ring element is introduced, the width of the feed decreases according to equation 2.1.2:

$$L_n = 0.8^n * W_f \qquad \text{Eqn. 2.1.2}$$

The ARR antenna is the most important part of the antenna design, as it contributes most significantly to increasing the bandwidth over what could be achieved with standard patch antennas.

2.1.3. ARR Disc Antenna

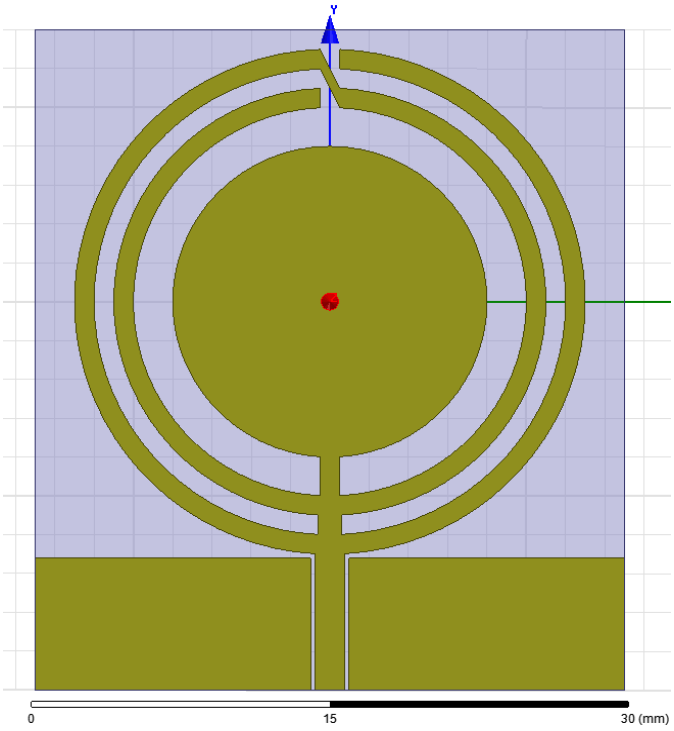

Figure 2.1.3 – ARR Disc Antenna

Combining the feed, taper, parasitic patches, disc and anisotropic ring resonator, provides the final antenna design demonstrated in figure 2.1.3; an anisotropic ring resonator disc antenna. As discussed in the next chapter, the ARR disc antenna is not only the aggregate of its visual constituents, but a constructive combination of its lesser parts. In simulation, the ARR disc antenna yields a near-toroidal radiation pattern from approximately 0 - 4 GHZ. The overall frequency reception determined by a combination

of the voltage standing wave ratio (VSWR) and return loss (S11) of the antenna is simulated to range from approximately 0 - 32 GHz. However in contrast to the simulation results, measurements indicate a dual band operation with an effective -10 dB return loss magnitude at 6.3 - 7.5 GHz and 8.4 - 9.5 GHz.

2.2. Substrate

2.2.1. FR-4

The substrate used in this design was a single-sided half ounce copper cladded FR-4 glass reinforced epoxy laminate sheet. FR-4 is currently the most widely used laminate in the world due to its decent thermal and electrical properties. It has a coefficient of thermal expansion of $1.4 \times 10^5/K$ a relative permittivity of 4.4 at 10GHz and a loss tangent of .02 at 10GHz. The substrate is made of woven fiberglass that uses an epoxy resin adhesive which is flame retardant; hence, “FR”. 4 is the designation for the quality of glass woven into this flame resistant final product.

Another reason for selecting FR-4 as the antenna substrate is due to wide-banding considerations. A key design factor regarding to the substrate when making a wide-band patch antenna is to use thick substrates with a low dielectric constant. FR-4, although only providing a relative permittivity of 4.4, provides one of the thickest laminate substrates available (1.6 mm).

2.3. Wide-Banding Techniques

A variety of wide-banding techniques borrowed from Lee et al. [2] have been implemented in the design of the ARR disc antenna. Although the impedance bandwidth of the antenna is already significantly broadband, other various techniques could have been employed to further broaden the antenna's useable spectrum. The three methods adopted here are the use of thicker dielectric substrates, edge-coupled or coplanar parasitic patches and slotted antenna designs.

Referring to Table 2.3.1, for commercialized mobile communication systems, the impedance bandwidths are relatively narrow and ranging from 7% to 13%. For ultra-wide bandwidth communication systems, it is as high as 109%. Achieving these bandwidths with patch antennas is theoretically possible with proper wide-banding techniques.

A grounded microstrip patch antenna in the form of a conducting patch is inherently narrow-band. This problem has been overcome over the last decade employing a number of techniques to improve the bandwidth of the microstrip patch antenna.

Through the introduction of slots and parasitic elements such as the anisotropic ring resonator and impedance-correction patches, additional resonances may be introduced to the antenna so that together with the main resonance of the conducting patch (in this case a disc antenna) a much broader bandwidth may be achieved.

Thicker substrates of lower permittivities are also beneficial in achieving a broader bandwidth, however with the introduction of thicker substrates, impedance mismatches are often introduced. Hence, the parasitic patches placed along the feed of

the ARR Disc antenna serve the purpose of both introducing additional resonances to broadband the return loss and correct impedance mismatches introduced via the use of thicker substrate.

System	Operating Frequency	Overall Bandwidh
Advanced Mobile Phone Service (AMPS)	Tx: 824-849 MHz	70 MHz (8.1%)
	Rx: 869-894 MHz	
Global System for Mobile Communications (GSM)	Tx: 880-915 MHz	80 MHz (8.7%)
	Rx: 925-960 MHz	
Personal Communications Service (PCS)	Tx: 1710-1785 MHz	170 MHz (9.5%)
	Rx: 1805-1880 MHz	
Global System for Mobile Communications (GSM)	Tx: 1850-1910 MHz	140 MHz (7.3%)
	Rx: 1930-1990 MHz	
Wideband Code Division Multiple Access (WCDMA)	Tx: 1920-1980 MHz	250 MHz (12.2%)
	Rx: 2110-2170 MHz	
Universal Mobile Telecommunication Systems (UMTS)	Tx: 1920-1980 MHz	250 MHz (10.2%)
	Rx: 2110-2170 MHz	
Ultra-wideband (UWB) for communications and measurement	Tx: 3100-10600 MHz	7500 MHz (109%)
	Rx: 3100-10600 MHz	

Table 2.3.1. – Frequencies of Wireless Communication Systems

2.3.1. Frequency Bands Associated with Wireless Communication

The table above shows the transmission and frequency bands allocated to wireless communication systems for the United States as well as some globally designated communication spectrum. Because these frequency bands are used almost exclusively for communication purposes with the exclusion of the ultra-wideband for communications and measurement, there is a high demand for antennas suited for these bandwidths. It is worth noting that many antennas developed for these applications are often of a dual-band or broadband nature as an offset is placed between transmission and reception frequencies to limit interference and preserve signal integrity [2].

3. Software

In this chapter, the various software programs used to model and simulate the ARR antenna are discussed briefly. An exploration of the electromagnetic simulator, electrical simulator and data plotting program used in the antenna simulation is provided.

3.1. Simulation and Data Analysis

The programs discussed in this section are intended for electromagnetic simulation of two or three dimensional structures. Using these tools, useful behaviors such as antenna radiation, return loss and other characteristics may be observed. Plotting this data is normally achieved using the data plotter included with the simulator. However, in order to improve plot quality, most data is presented using Veusz, a stand-alone plotting program.

3.1.1. ANSYS High Frequency Structure Simulator

The ANSYS High Frequency Structure Simulator (HFSS) is a complete three dimensional finite-element-method solver. Originally developed specifically for antenna simulation, this program contains an antenna designer's dream toolbox. Between RCS

plotting, return loss, radiation patterns and much more, HFSS offers a wonderful tool for modeling and simulating three dimensional electromagnetic structures.

3.1.2. Agilent Advanced Design System 2013

The Agilent Advanced Design System (ADS) is the industry standard in RF engineering. With its two-dimensional graphical design interface, designing complex structures is quick and straight-forward. With assisted features such as “smart-snap” placement of lines and shapes and user-defined layer stack-up, three dimensional structures may be drawn with ease in ADS. This 3D design platform chooses material thicknesses beforehand, allowing users to only worry about two dimensional design of any object. This simplicity is exactly why ADS is the industry standard in layout design.

3.1.3. Veusz Data Plotter

Veusz data plotter is a free program available online which may be used to import and plot data from external sources. The touchstone file format was consistently used to save and store performance data of antenna simulations. Veusz offers a very aesthetically appealing and user-friendly medium for uploading and plotting touchstone files.

3.1.4. Agilent Physical Layer Test System 2013

Agilent Physical Layer Test System (PLTS) is a signal integrity tool used to measure scattering parameters through the use of an Agilent-based network analyzer.

Agilent PLTS was used to make and record measurements as well as export results in a touchstone file format for plotting in Veusz.

4. Antenna Model & Dimensions

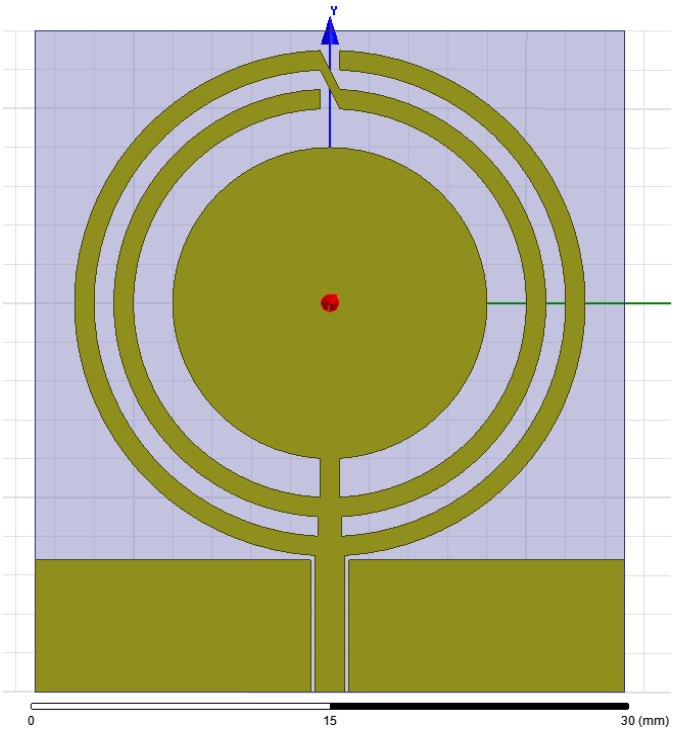

Fig. 4.1 - ARR Disc Antenna - Top View

4.1. ARR Disc Antenna

Figure 4.1 depicts a top view of the proposed patch antenna design. It is a monopole antenna with a central line feed. The feed of the antenna consists of a logarithmic taper sized according to equation 2.1.2 presented earlier in the thesis. This

tapered feed also parasitically couples to the rectangular patches seen on the bottom of the ARR disc antenna design. As can be seen in figure 4.1, the tapered feed decreases in width as each of the rings comprising the anisotropic ring resonator emanate from the feed.

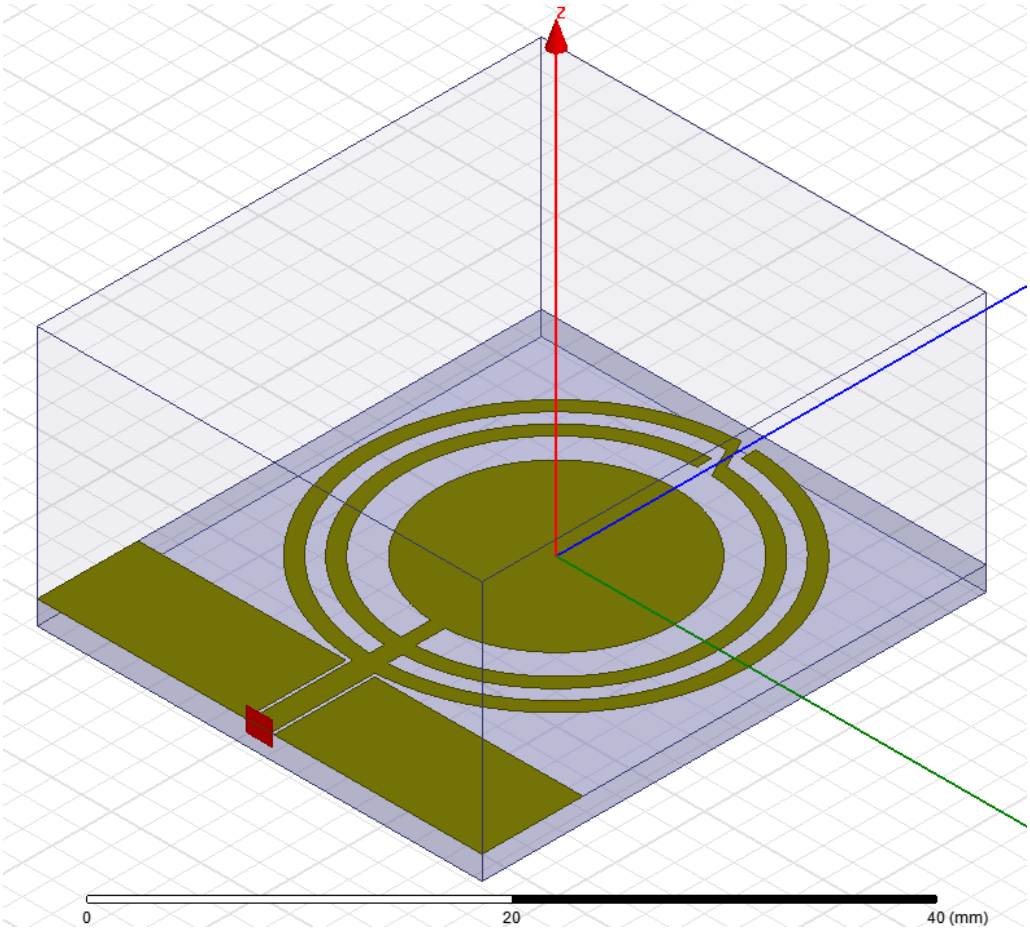

Fig. 4.2 - ARR Disc Antenna - Diagonal View

4.2. ARR Disc Antenna – Diagonal View

A diagonal view of the patch antenna design is shown above in figure 4.2. The small rectangular element shown in red to the left of the figure is the wave port used as the current source. The current from this source propagates throughout the structure shown above first through the tapered feed, coupling with the rectangular parasitic patches, then through the rings of the antenna and eventually through the disc of the antenna.

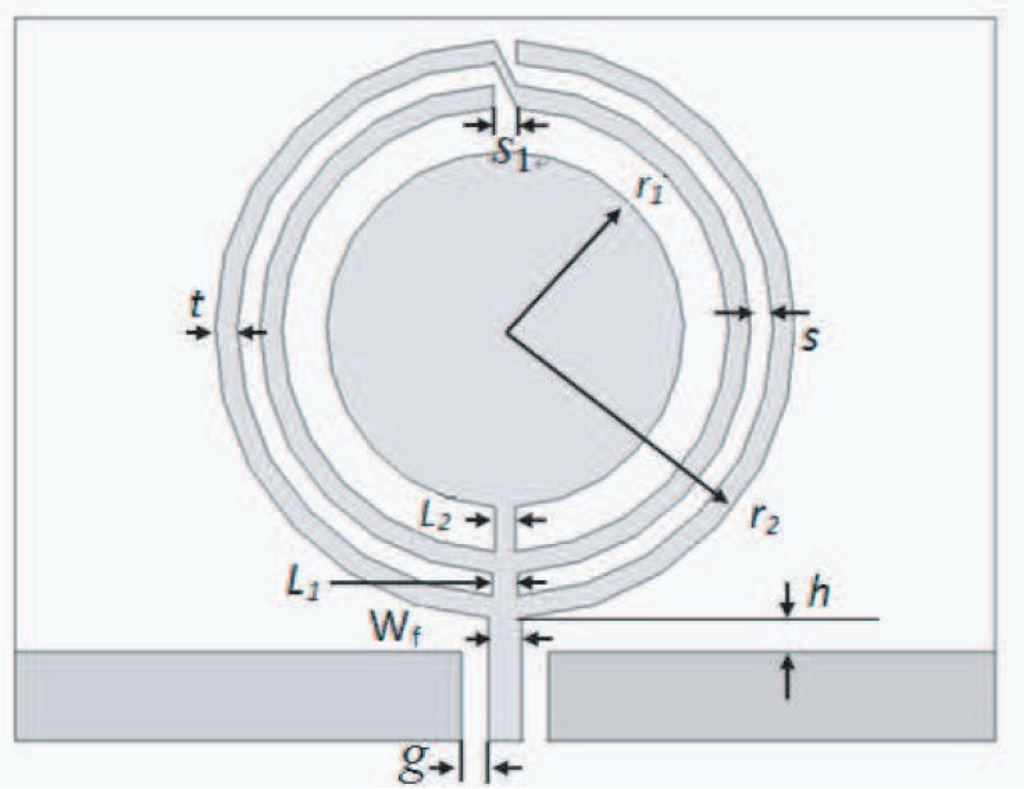

Fig. 4.3 - ARR Disc Antenna – Dimension Diagram

W_f	g	r_1	r_2	t	s	s_1	h
1.5 mm	.22 mm	8 mm	13 mm	1 mm	1 mm	1 mm	.2 mm

Table 4.3 – Table of antenna dimensions

$$L_n = 0.8^n * W_f$$ Eqn. 4.3

4.3. ARR Disc Antenna – Dimensions

The dimensions of the proposed patch antenna are listed in table 4.4 shown above. The corresponding locations for the dimensions of the antenna are shown in figure 4.3.

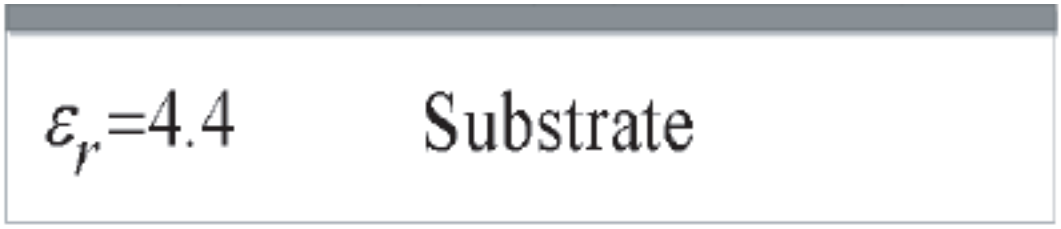

Fig.4.5 – Substrate Dimensions

4.5. Substrate Dimensions

The substrate used for the proposed patch antenna is a FR-4 fiber glass reinforced epoxy laminate. The availability of FR-4 makes the fabrication of this structure relatively low cost while providing a thick substrate, desired for wide-banding purposes as mentioned in section 2.3. In addition to providing a substrate thickness of 1.6 mm, FR-4 has a relative permittivity of approximately 4.4 at a test frequency of 10GHz. For the purpose of this antenna design, an FR-4 substrate with a half-ounce of single-sided copper cladding was used. A half ounce of copper cladding has a thickness of approximately 18 um.

5. Simulation Results

5.1. Disc Antenna with Coplanar Parasitic Patches

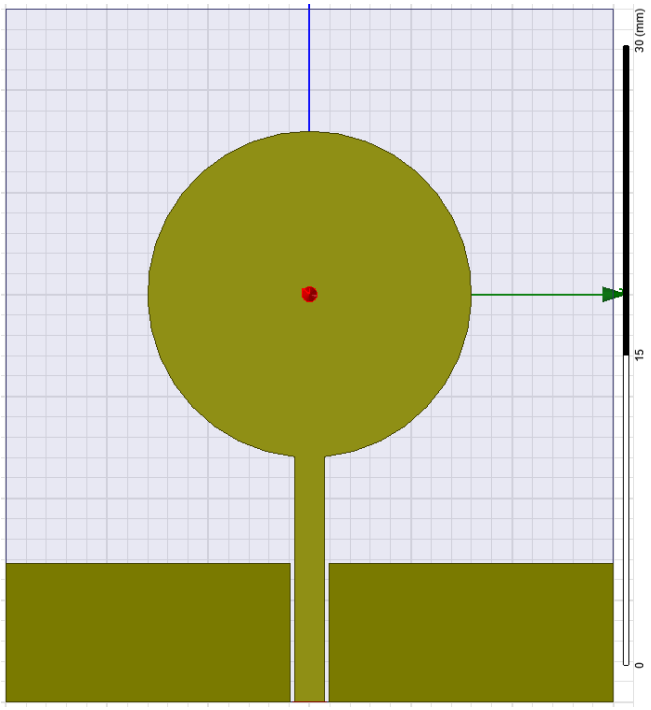

Figure 5.1.1 – Disc antenna with parasitic patches – Top View

5.1.1. Disc Antenna with Parasitic Patches

In order to understand how the theoretical broadband structure of the ARR disc antenna works, the overall antenna design has been simplified into its constituent parts. Shown in figure 5.1.1 is a top view of a monopole disc antenna with rectangular parasitic

patches along the feed. The simulated performance of this structure is shown in figure 5.1.3.

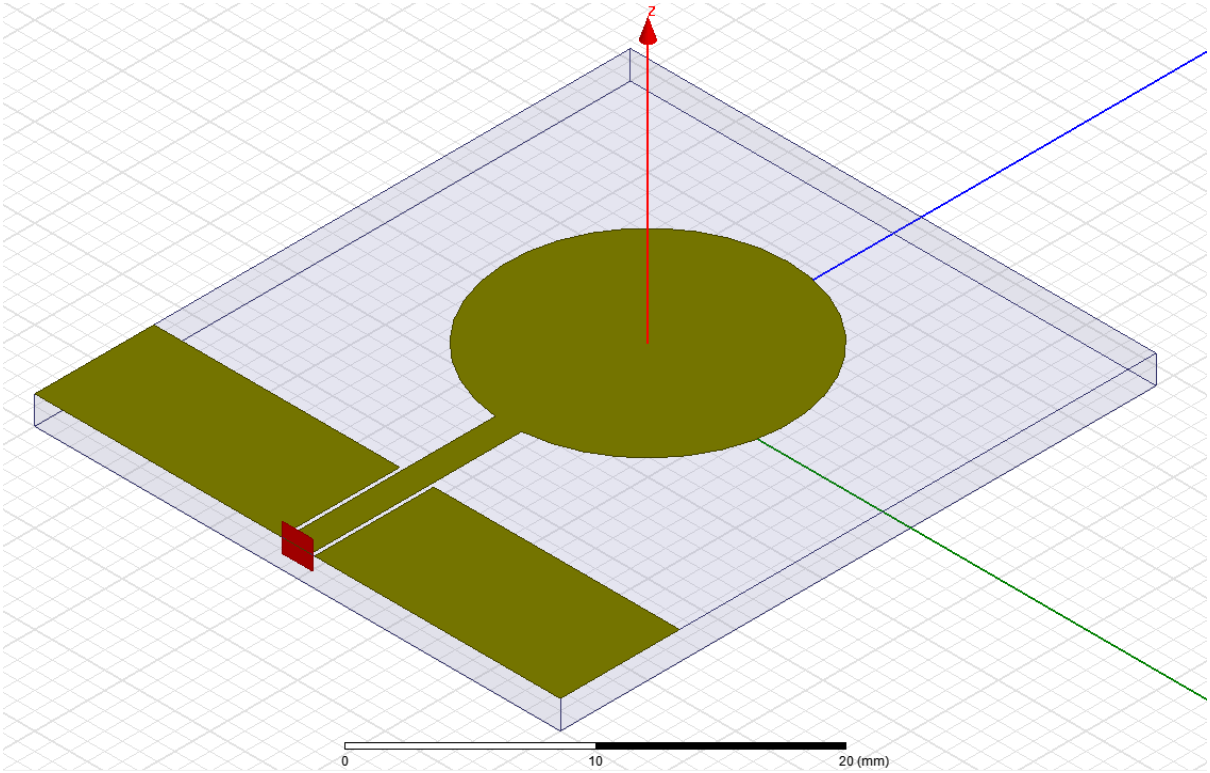

Figure 5.1.2 – Disc antenna with parasitic patches – Diagonal View

5.1.2. Disc Antenna with Parasitic Patches – Diagonal View

Figure 5.1.2 offers an alternative view of the circular disc antenna with rectangular parasitic patches included. The disc and parasitic elements are provided in this section separate from the rest of the antenna design in order to verify the overall antenna operation as a sum of already proven antenna design techniques including the disc antenna and rectangular patches as shown in figure 5.1.2.

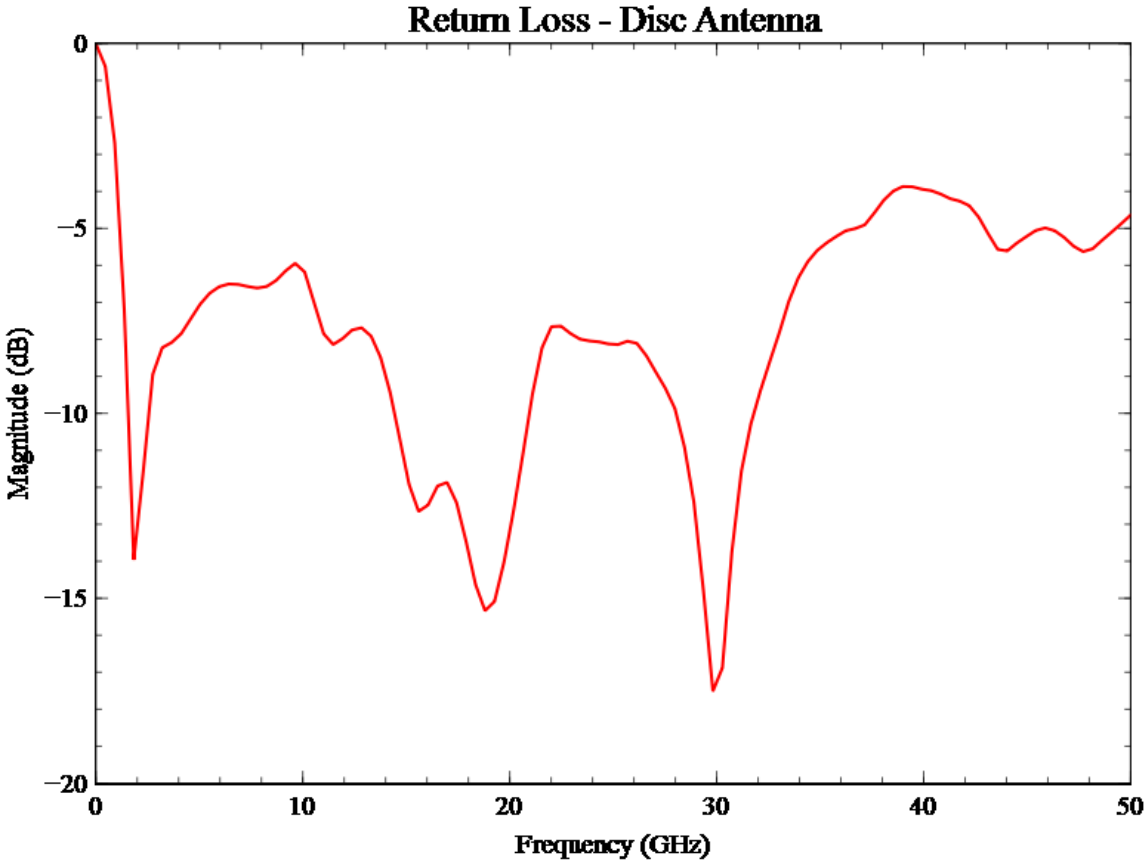

Figure 5.1.3 – Disc antenna with parasitic patches – Return Loss

5.1.3. Disc Antenna with Parasitic Patches – Return Loss

The simulated operation of the disc antenna along with the rectangular patches exhibit behavior we expect to see from such a structure. Circular patches provide a single resonance, seen at approximately 30 GHz in the return loss shown in figure 5.1.3. The rectangular patches also perform as they should, exhibiting a resonance associated with the width of the patch and another resonance associated with the length of the rectangular

patch. These resonaces are observed at approximately 15 GHz and 19 GHz in the plot provided in the figure above.

5.2 Anisotropic Ring Resonator Antenna

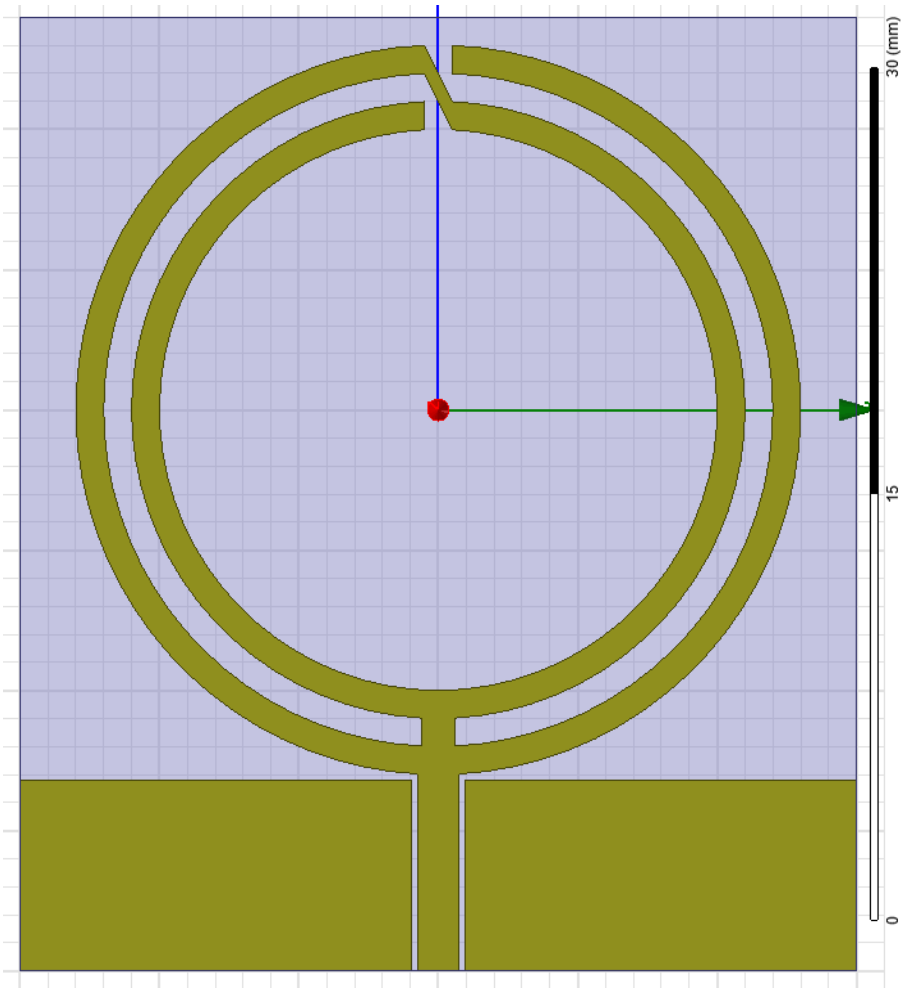

Figure 5.2.1 – ARR antenna with parasitic patches – Top View

5.2.1. ARR antenna with parasitic patches

The novel part of this antenna design is the anisotropic ring resonator. With a customized tapered feed that gradually decreases in width according to equation 4.1, the feed is designed to provide an impedance of approximately 50 ohms. As observed in

figure 5.2.3, the ARR is theorized to contribute greatly to the wide-banding of the antenna.

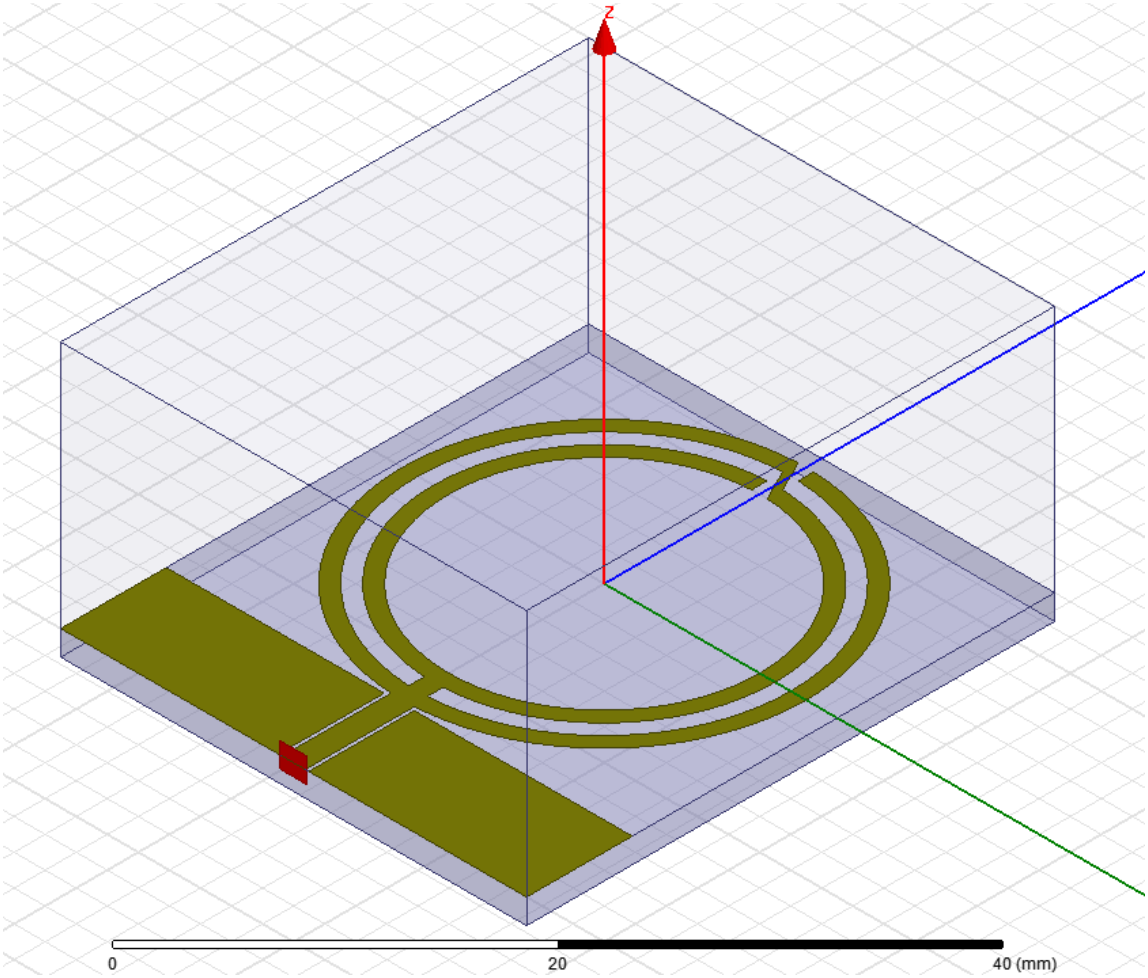

Figure 5.2.2 – ARR antenna with parasitic patches – Diagonal View

5.2.2. ARR antenna with parasitic patches – Diagonal View

Figure 5.2.2 offers an alternative view of the anisotropic ring resonator. The parasitic rectangular patches are kept in the design of the antenna to widen the useable bandwidth of the antenna. Because the parasitic patches are edge-coupled to the main

antenna structure, minimal considerations need to be made with regards to impedance matching.

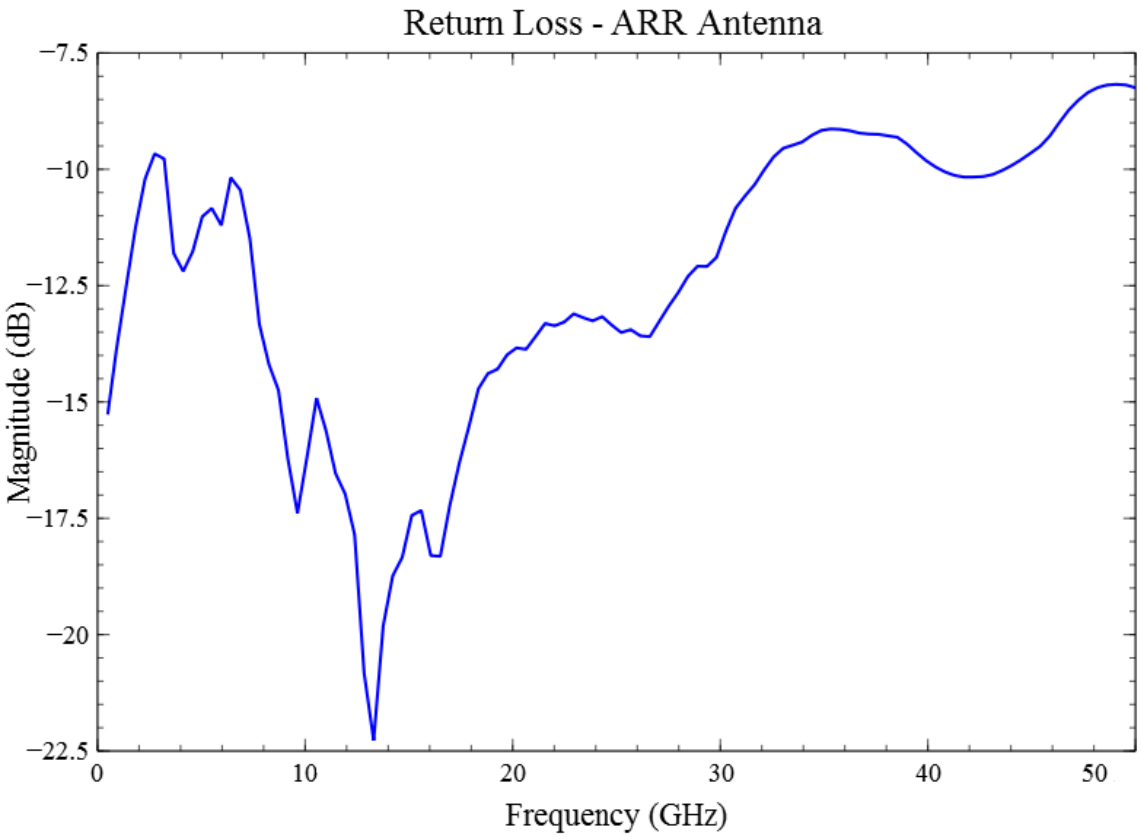

Figure 5.2.3 – ARR antenna with parasitic patches – Return Loss

5.2.3. ARR antenna with parasitic patches – Return Loss

The simulated return loss of the anisotropic ring resonator antenna is observed in figure 5.2.3. Yielding a remarkable useable impedance bandwidth, it can be assumed that according to the simulated data shown in figure 5.3.3, the ARR makes the most

significant contribution to broadening the bandwidth of the simulated ARR disc antenna as a whole.

5.3 ARR Disc Antenna

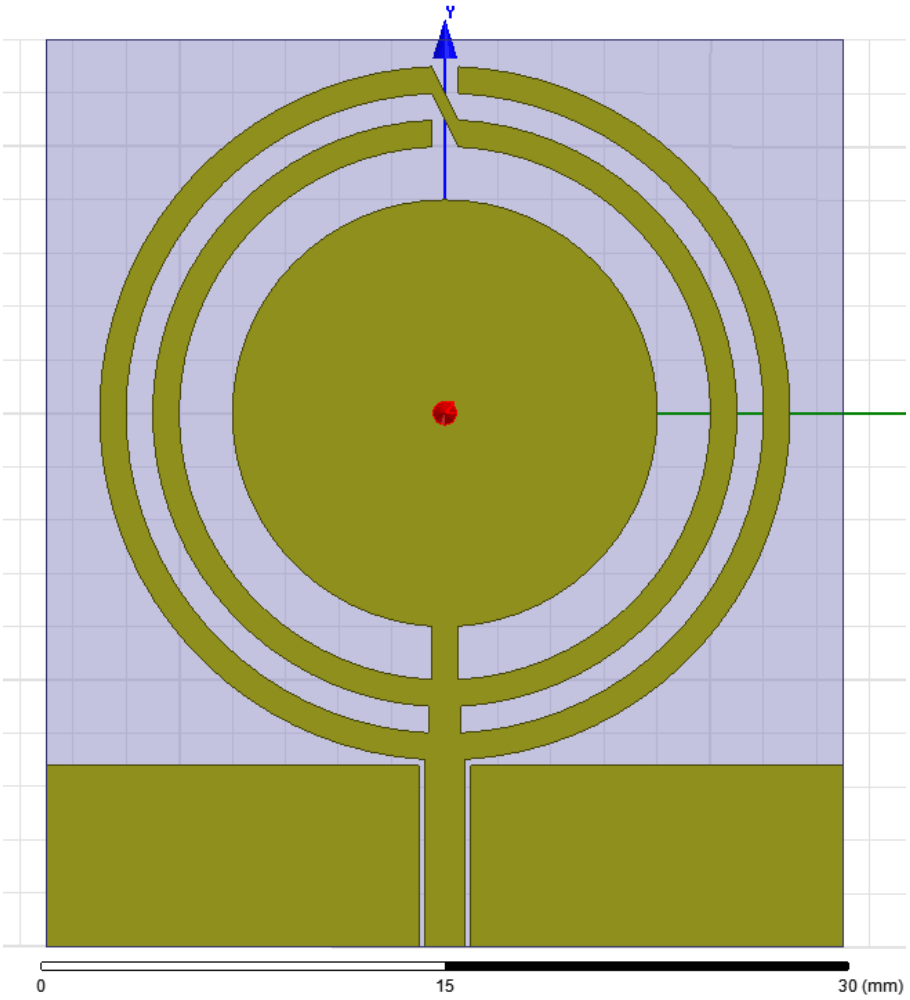

Figure 5.3.1 – ARR disc antenna with parasitic patches – Top View

5.3.1. ARR disc antenna with parasitic patches

The final design of the ARR disc antenna is shown in figure 5.3.1. All reviewed parts including the tapered feed, parasitic rectangular patches, circular disc and anisotropic ring resonator are included in this design and its simulated S11 may be observed in figure 5.3.3.

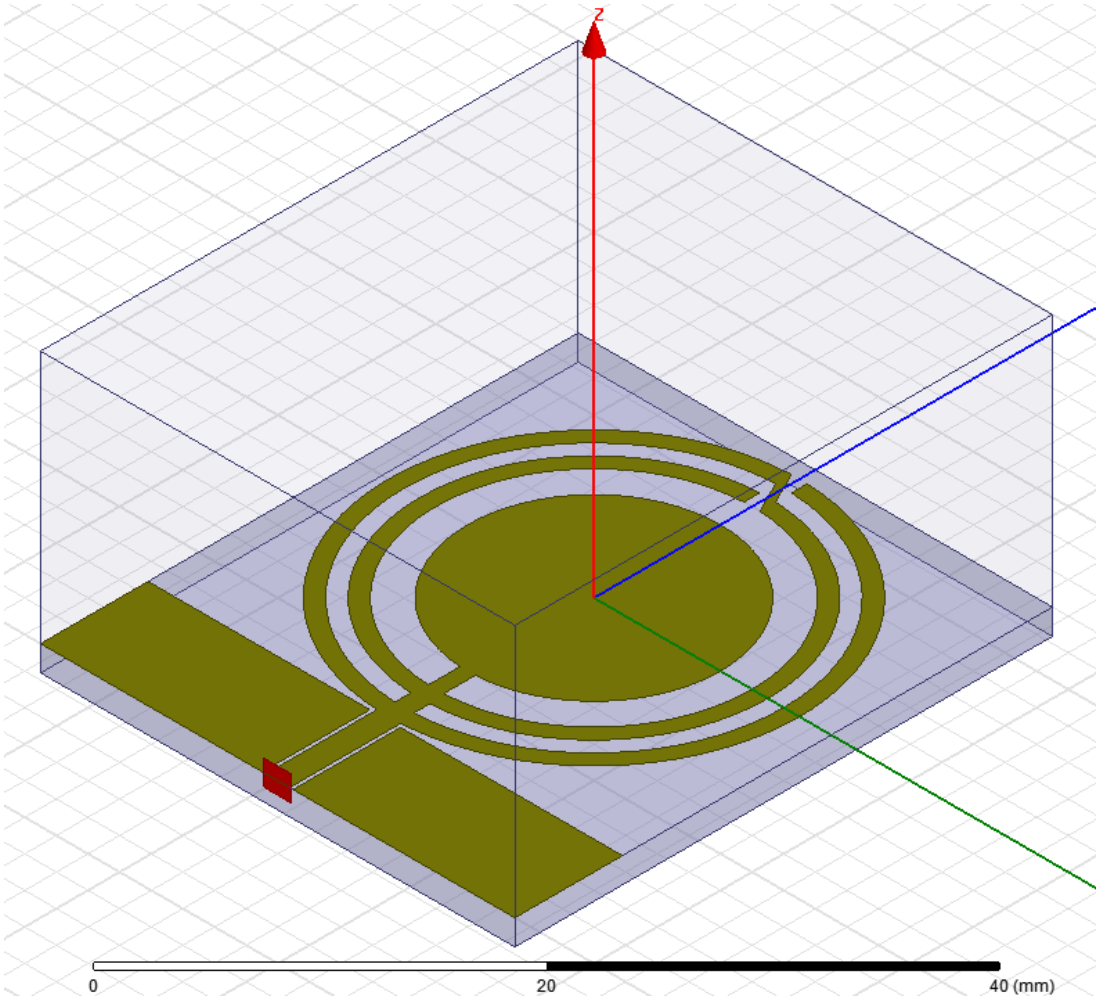

Figure 5.3.2 – ARR disc antenna with parasitic patches – Diagonal View

5.3.2. ARR disc antenna with parasitic patches – Diagonal View

An alternative view of the final antenna design is presented in figure 5.3.2. The overall size of the antenna is less than 40 mm, yet simulates a useable impedance bandwidth including lower frequency bands typically associated with larger antenna designs.

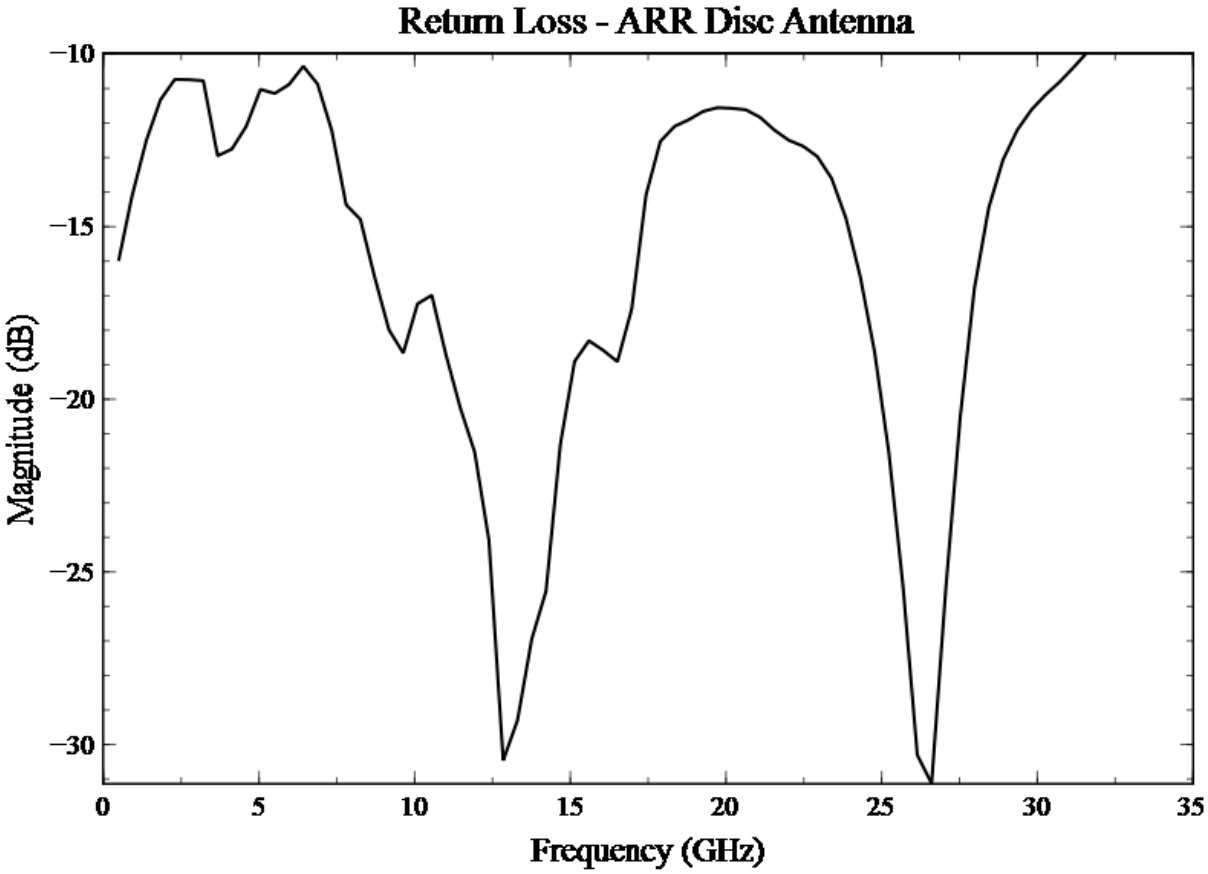

Figure 5.3.3 – ARR disc antenna with parasitic patches – Return Loss

5.3.3. ARR disc antenna with parasitic patches – Return Loss

The simulated return loss of the ARR disc antenna and its parasitic rectangular patches is provided in figure 5.3.3. Observing the S11 of the proposed antenna, it presents a constructive combination of the return loss associated with the resonance of the circular disc antenna with parasitic rectangular patches seen in figure 5.1.3 and the simulated return loss of the ARR antenna with parasitic rectangular patches observed in figure 5.2.3.

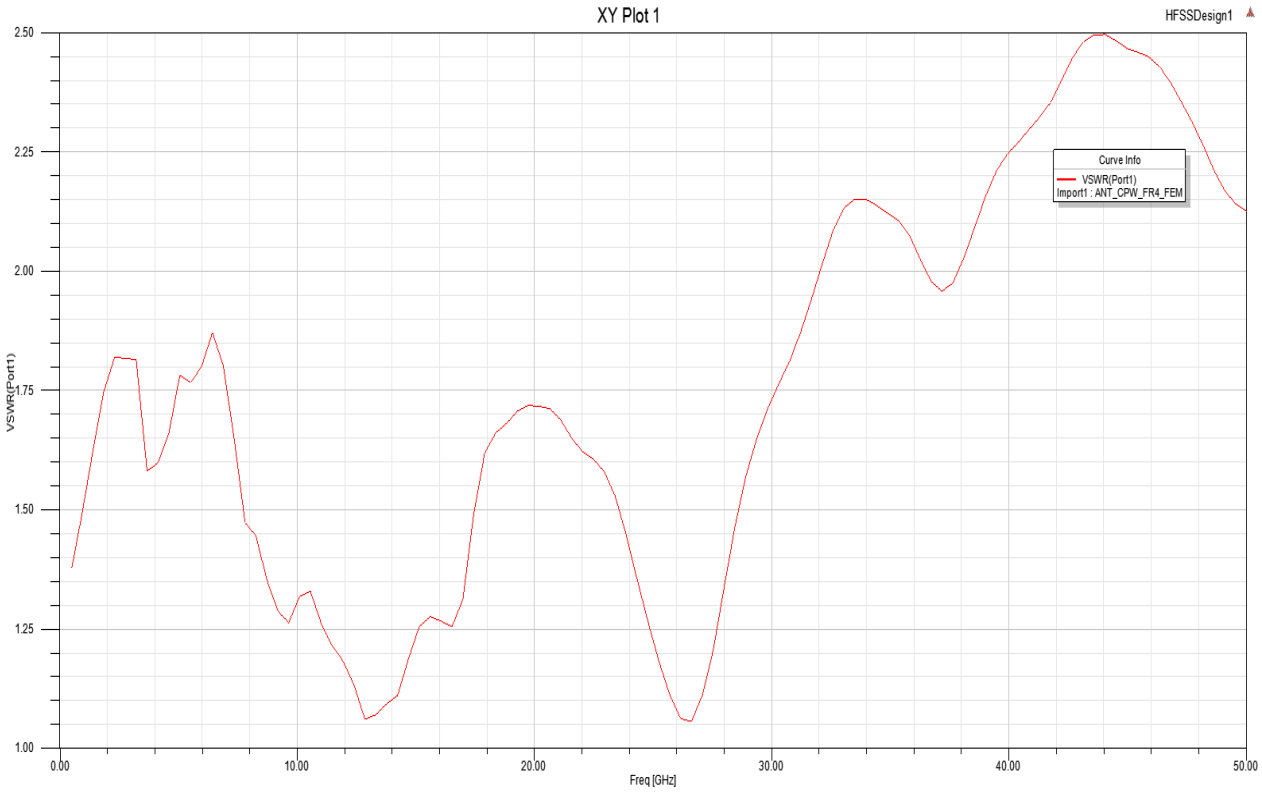

Figure 5.3.4 – ARR disc antenna with parasitic patches – VSWR

5.3.4. ARR disc antenna with parasitic patches – VSWR

Using HFSS, the simulated voltage standing wave ratio of the ARR disc antenna with parasitic rectangular patches is demonstrated in figure 5.3.4. Similar to obtaining a useable impedance bandwidth associated with the -10 dB magnitude of the antenna's return loss, it is assumed frequencies with voltage standing wave ratios below a ratio of 2 are adequate for signal reception and transmission from the simulated antenna. From the figure above, it is confirmed that our return loss and voltage standing wave ratio match correctly across the same useable frequency range.

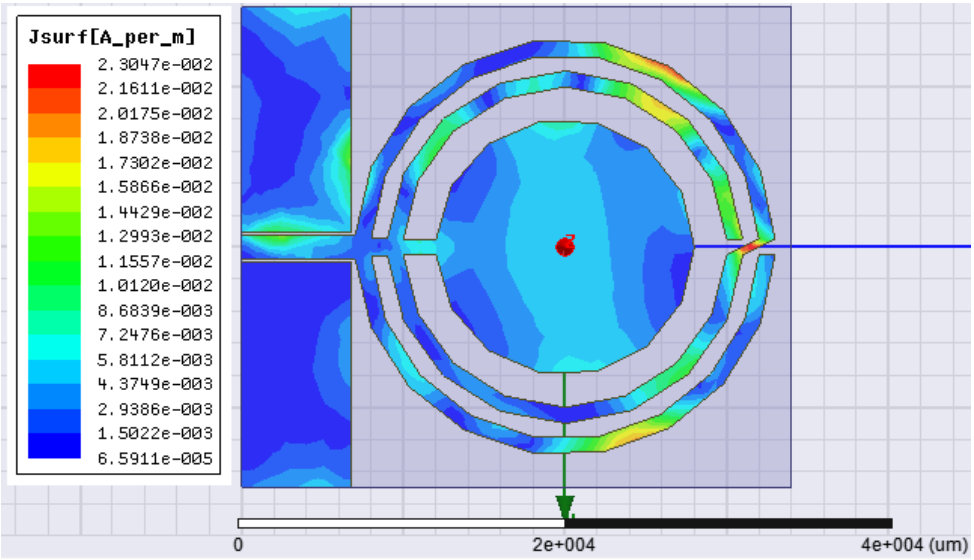

Figure 5.3.5 – ARR disc antenna with CPP's Surface Current Distribution at 13 GHz

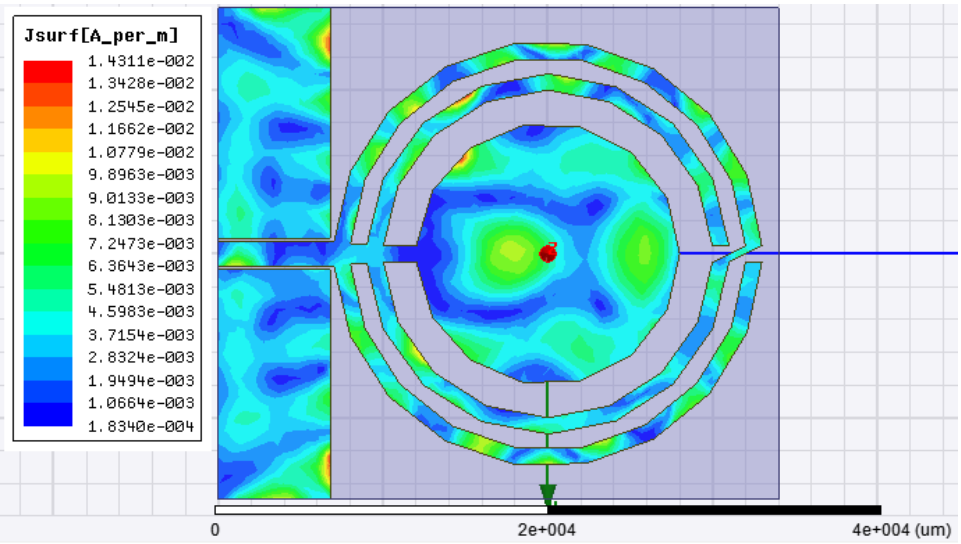

Figure 5.3.6 – ARR disc antenna with CPP's Surface Current Distribution at 26.5 GHz

5.3.6. ARR disc antenna with coplanar parasitic patches – Surface Current Distributions

Observing the simulated surface currents of the ARR disc antenna and its parasitic rectangular patches at its two strongest resonant frequencies, it may be inferred that the anisotropic ring resonator performs a larger role at 26.5 GHz than 13 GHz.

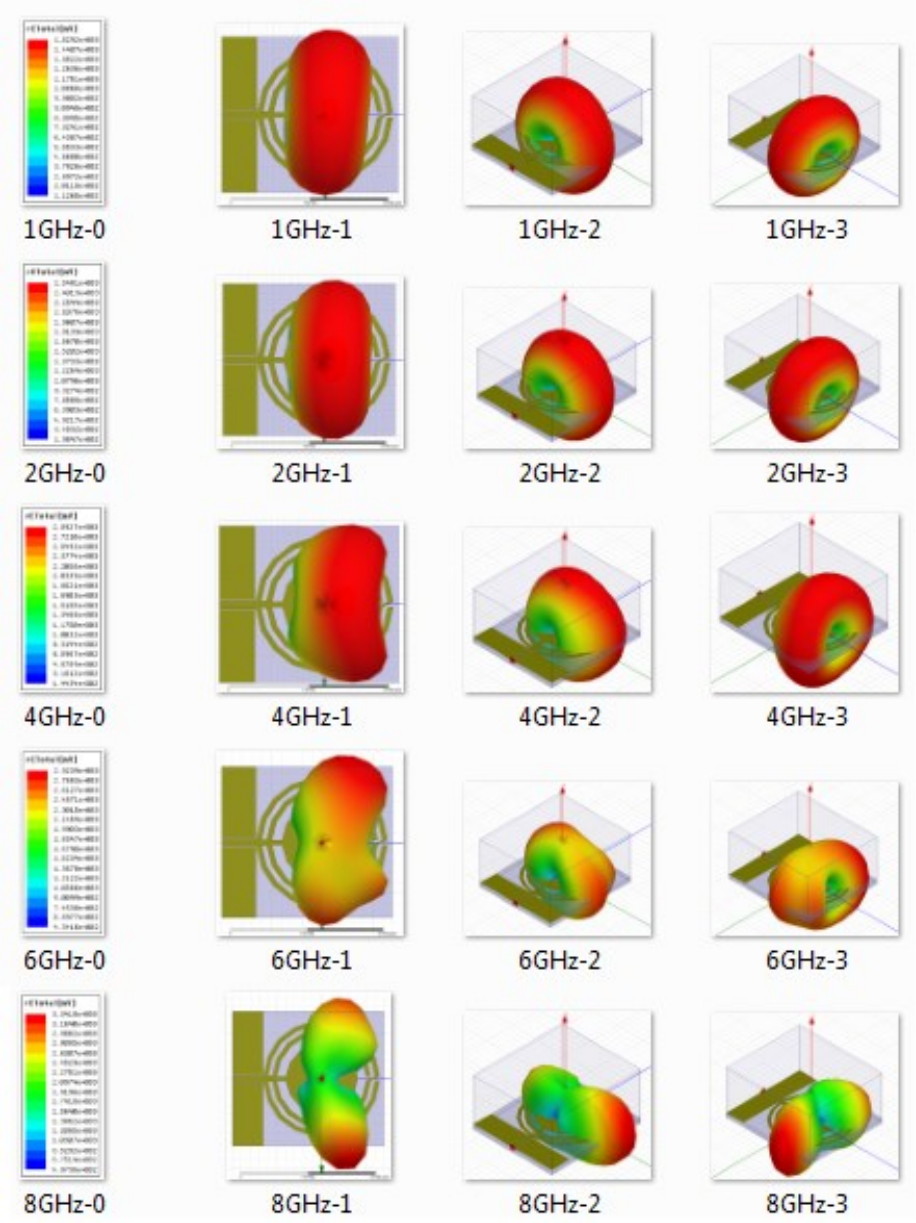

Figure 5.3.7 – ARR disc antenna with parasitic patches – Radiation Sweep

5.3.7. ARR disc antenna with parasitic patches – Radiation Sweep (1GHz-8GHz)

Over a range of 1GHz to 4GHz, a nearly toroidal radiation pattern is demonstrated.

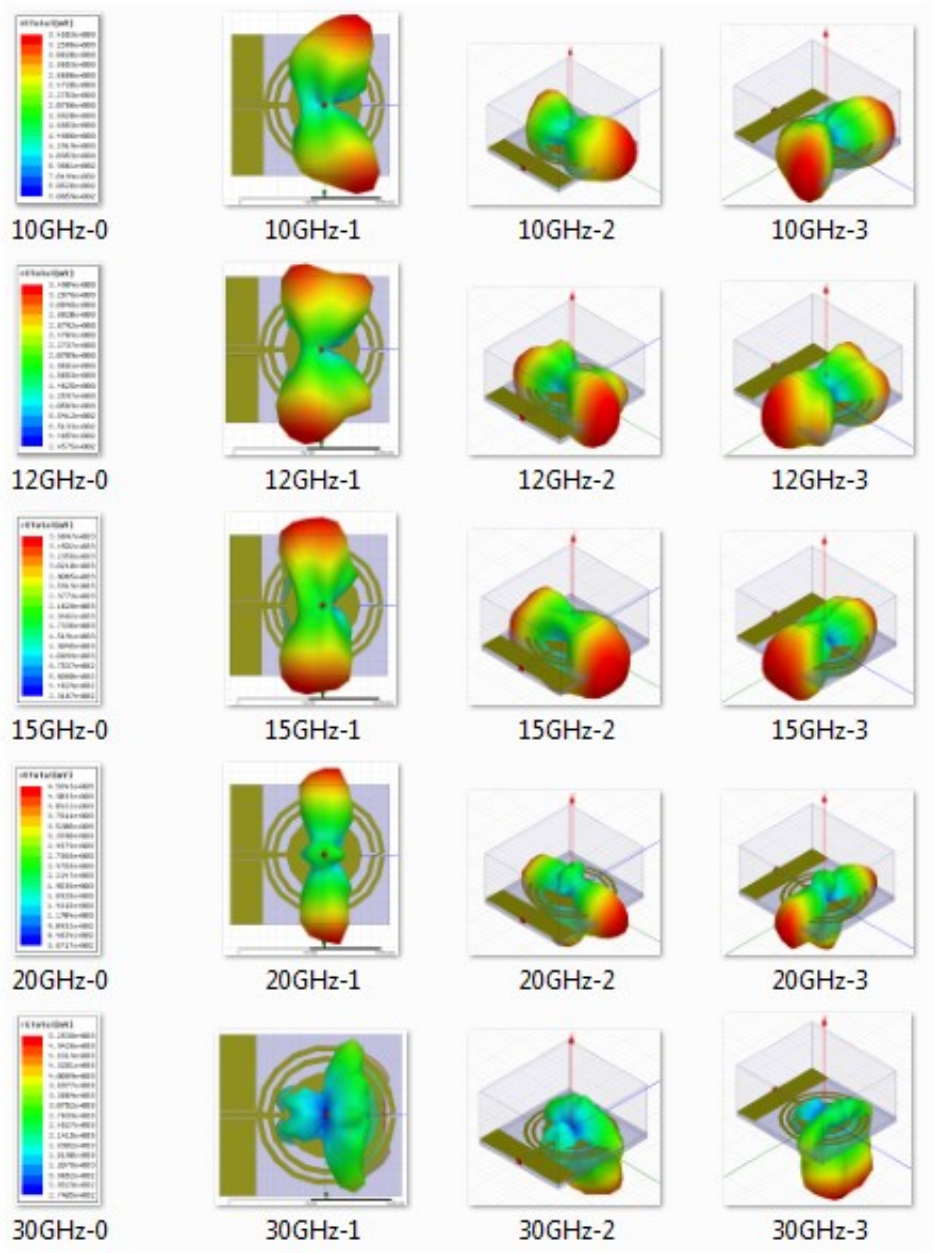

Figure 5.3.8 – ARR disc antenna with parasitic patches – Radiation Sweep (Cont'd.)

5.3.8. ARR disc antenna with parasitic patches – Radiation Sweep (10GHz-30GHz)

Over a range of 10GHz to 30GHz, mostly unusable and modal radiation is observed.

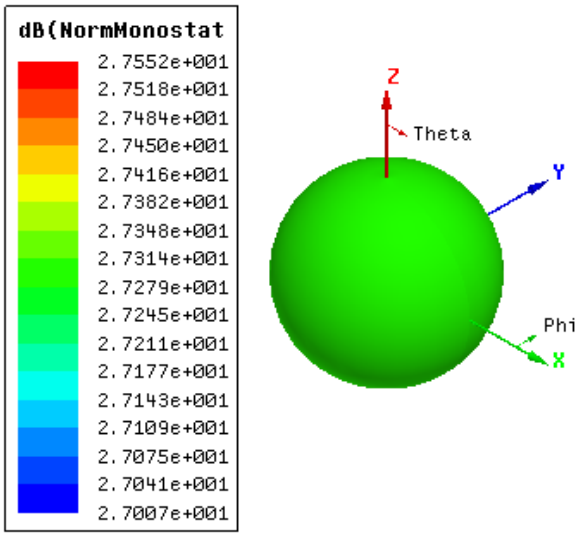

Figure 5.3.9 – Monostatic Radar Cross Section at 26.5 GHz

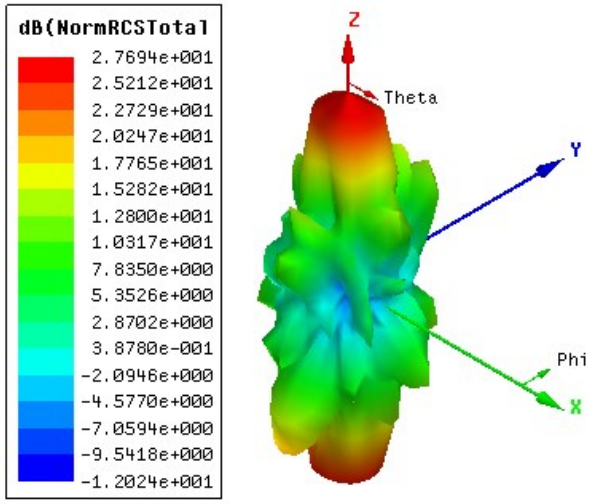

Figure 5.3.10 – Bistatic Radar Cross Section at 26.5 GHz

5.3.10. ARR disc antenna with parasitic patches – Radar Cross Sections (RCS)

Although at a frequency with a poor radiation pattern, the simulated mono-static RCS at 26.5 GHz seen in figure 5.3.9 behaves as an ideal metamaterial with regards to minimal re-radiation.

5.4 Comparison of Simulated Return Losses

Analyzing the return losses of the ARR disc antenna along with its constituent parts, we observe that the final product (ARR disc antenna) shown in black in figure 5.4.1 performs as a combination of its more basic parts including the disc antenna and ARR antenna, both of which also have impedance matching edge-coupled parasitic patches.

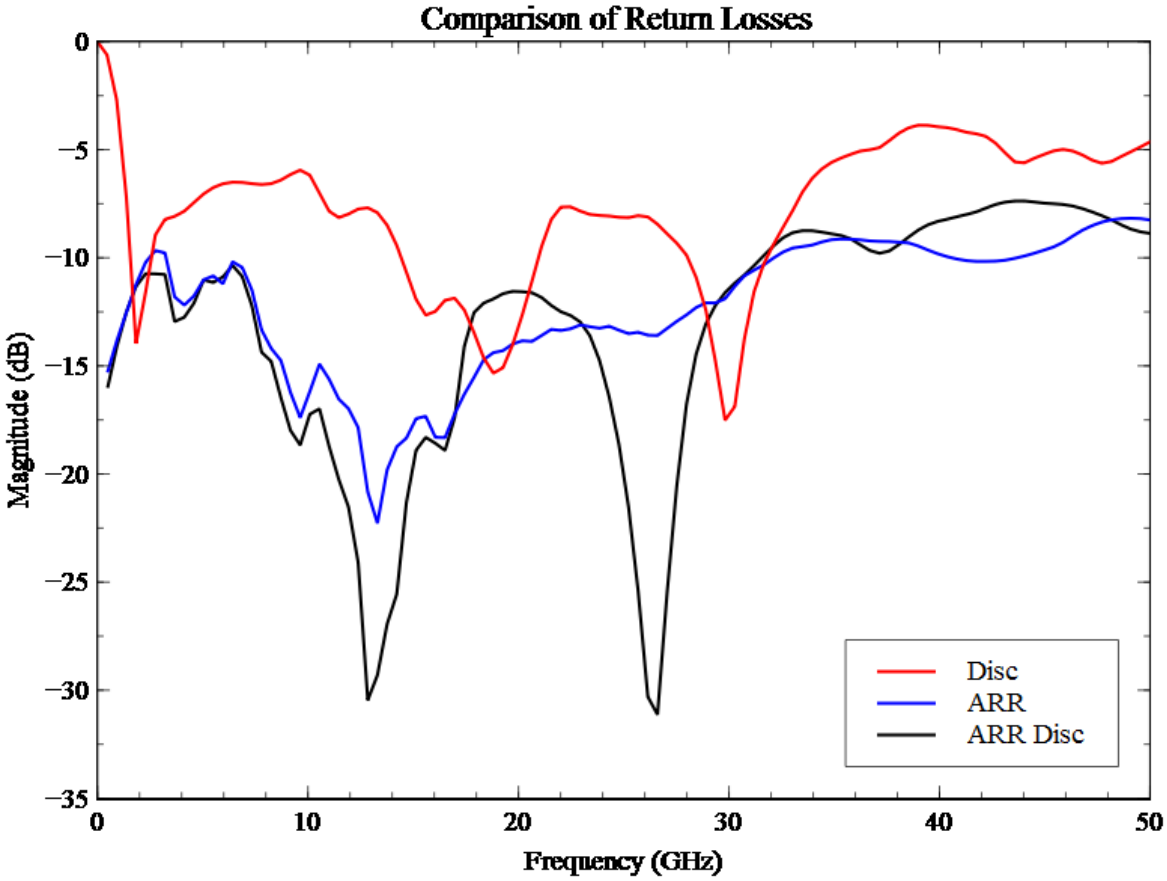

Figure 5.4.1 – Return losses of ARR disc antenna, ARR antenna and disc antenna (all with coplanar parasitic patches included)

6. Fabrication

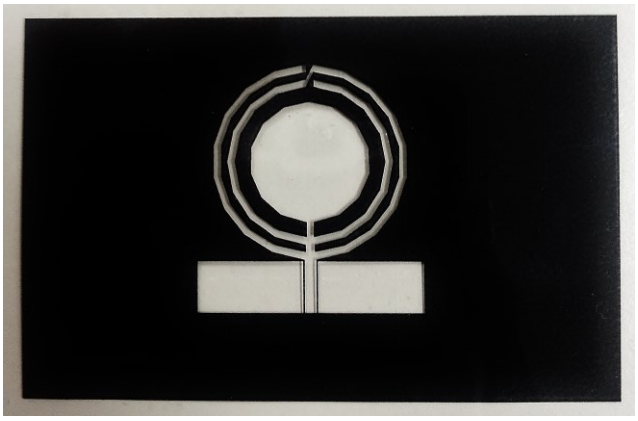

Figure 6.1 - Negative Transparency of Antenna Artwork

6.1. Negative Image Development

The first step in the fabrication process is to negatively develop the FR-4 copper clad board. Although many fabrication techniques involve the use of positively developed images, the Kepro bench-top developer available through Mr. Joe Haggerty of the Auburn University electrical engineering department utilizes a negative development technique and thus required the transparency placed above the copper-side of the FR-4 sample to be a negatively contrasted image of the artwork to be developed. This is shown in figure 6.1, as the clear region of the transparency designates the regions of the PC

board which retain copper cladding and the black regions indicate copper to be etched off the substrate.

Figure 6.2 – Kepro Bench-Top Developer

6.2. Kepro Negative Bench-Top Developer

The Kepro developer machine used to negatively develop the light-sensitized boards after the negative image of the artwork has been attached is shown in figure 6.2.

Figure 6.3 – Kepro Bench-Top Etcher

6.3. Kepro Bench-Top Etcher

In order to remove the unwanted copper cladding from the light-sensitized and developed board, the exposed sample of FR-4 is then placed in the Kepro etching machine seen in figure 6.3. Areas not exposed to lighting in the stages of development are removed from the board using a laser etch technique.

Figure 6.4 – Kepro Bench-Top Rinse Unit

6.4. Kepro Bench-Top Rinse Unit

After the board has been developed, unwanted chemical residue must be rinsed before being sent to the etcher. This rinse is done by the rinse unit shown in figure 6.4. Areas left with chemical residue may produce unwanted copper spots once etched. After etching, the board must once again go through an additional rinse cycle to remove the leftover residue left on the board from the etch cycle.

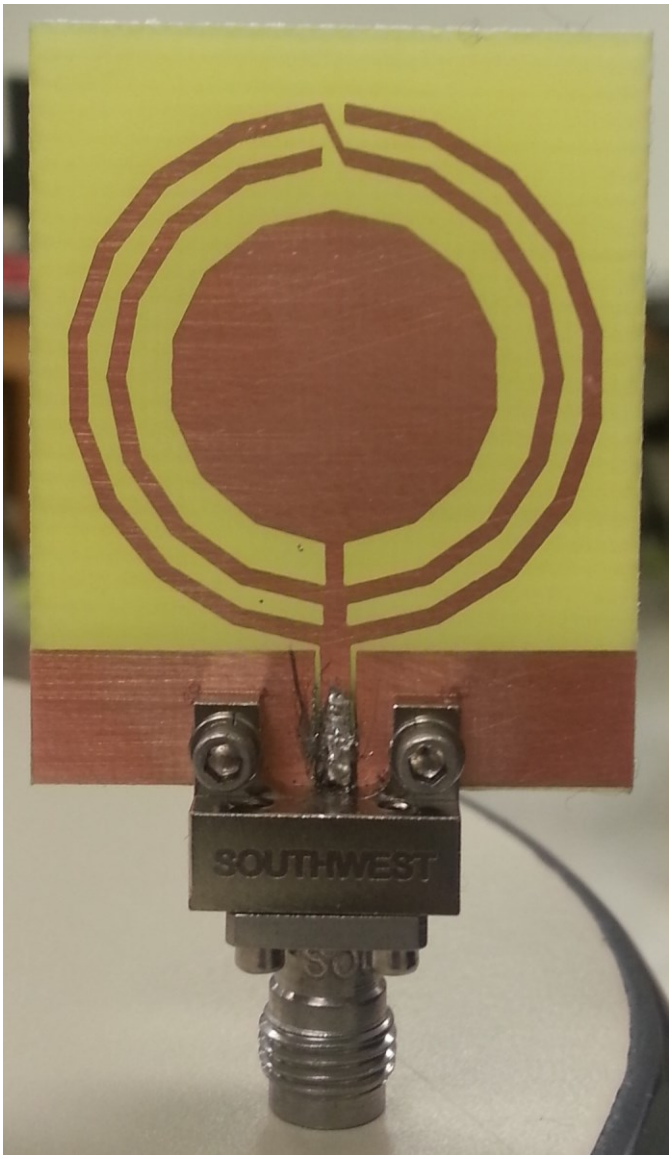

Figure 6.5 – Fabricated ARR Disc Antenna with CPP's and 2.4 mm Connector

6.5. Fabricated ARR Disc Antenna with CPP's and 2.4 mm End-Launch Connector

Once the copper cladded board has been developed, rinsed and etched, the excess substrate is cut using a guillotine blade. This part of the fabrication process may take a toll on the performance of the structure as the guillotine is operated by hand and flaws in

the symmetry of the antenna may appear due to human operation of the guillotine. Once cut to the desired dimensions, the board then had holes cut in the appropriate locations for the 2.4 mm end launch connector to be established. A Southwest Microwave 2.4 mm air-insulated connector was used to ensure reliable measurement up to 50 GHz. Once the connector was properly secured, the signal pin was soldered to the feed line of the antenna. The fully fabricated antenna design is shown in figure 6.5.

To demonstrate the relative size of the antenna, the antenna with connector attached is placed next to a U.S. quarter dollar as seen in figure 6.6.

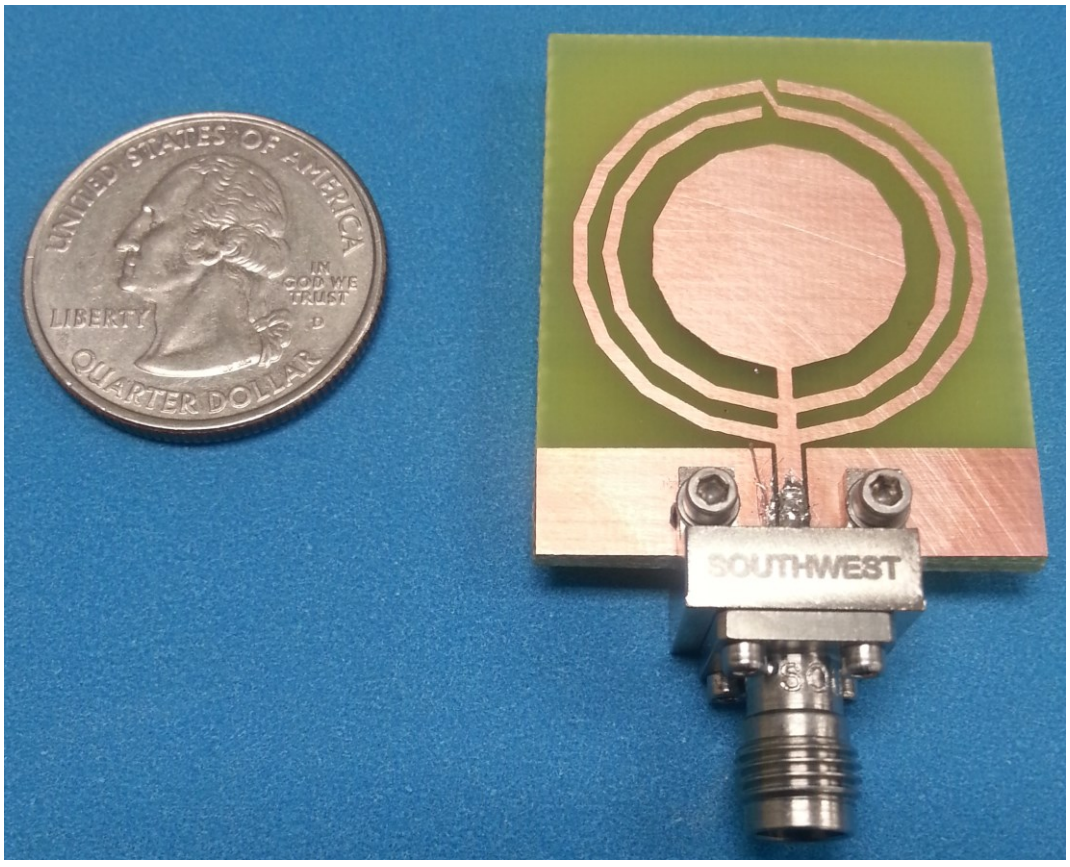

Figure 6.6 – Demonstration of Antenna's Relative Size

7. Measurements

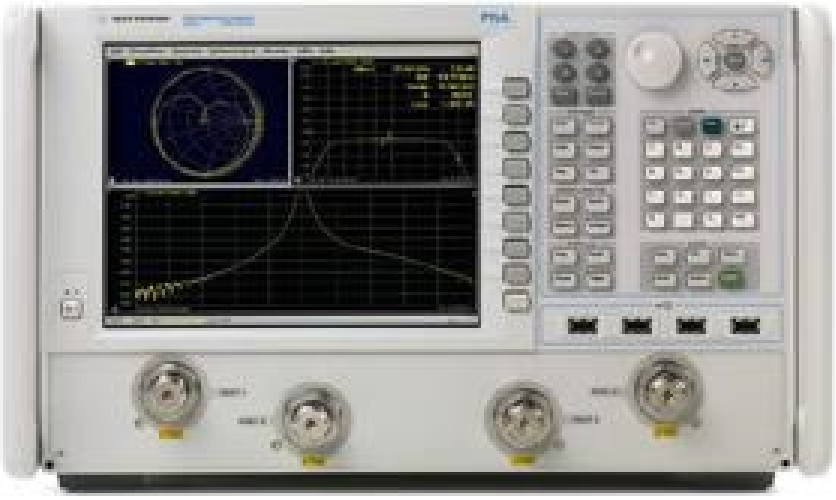

Figure 7.1 - Agilent N5227 Network Analyzer

7.1. Agilent N5227 Network Analyzer

To measure the fabricated antenna's scattering parameters, an Agilent N5227 network analyzer was used. The N5227, shown in figure 7.1, is the highest performance network analyzer available to date and is capable of measuring from 10 MHz to 67 GHz as well as 4-port measurements. For the antenna presented in this paper, the network

analyzer was more than sufficient as the antenna requires only a single-port measurement up to 35 GHz. A convenience associated with the N5227 is that the network analyzer is capable of exporting measurement results in a touchstone file format to later be plotted using Veusz. Frequency-domain measurements of the ARR disc antenna with parasitic rectangular patches and 2.4 mm end-launch connector taken with the network analyzer are provided in figure 7.2 below.

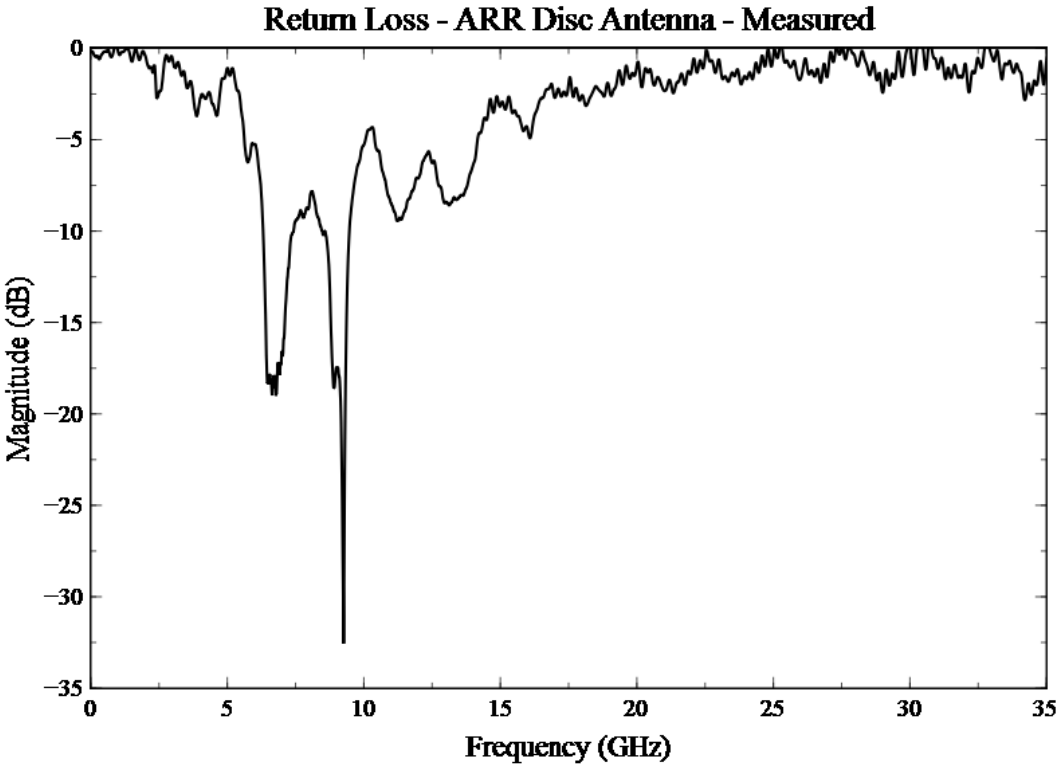

Figure 7.2 – Measured Return Loss of Antenna with 2.4 mm Connector

7.2. Measured Return Loss of ARR Disc Antenna with 2.4 mm Connector

Unfortunately, the measured scattering parameters obtained from the N5227 network analyzer do not correlate well with the simulated return loss observed in figure 5.3.3. Although the optimistic intention of the simulation results was to achieve a broadband antenna design, the measured return loss may yield some benefit. As mentioned in section 2.3.1, dual-band antenna designs are very popular amongst wireless communication devices and typically require a distinct separation between frequency bands so that transmit and receive channels of a device do not interfere with one another.

Observing the measured return loss demonstrated by the ARR disc antenna with coplanar parasitic rectangular patches in figure 7.2., such wireless communication applications operating in the previously mentioned frequency bands are a possibility. In addition, there is potential for further wide-banding of the measured return loss of the antenna as the magnitude between the strong resonant peaks located at 7 GHz and 9 GHz is near -10 dB.

8. Conclusion

According to simulation, the anisotropic ring resonator disc antenna demonstrated excellent broadband characteristics. Unfortunately, measurement results strongly contrasted the simulated return loss of the ARR disc antenna. Although the results did not match, S11 measurements proved the antenna to perform as a dual-band structure with strong return loss resonances less than -10 db from 6.3 GHz to 7.5 GHz and 8.4 GHz to 9.5 GHz. Its wideband characteristics were achieved by proved wide-banding techniques [2]. The addition of a metamaterial resonator and other various wide-banding techniques such as the use of thicker substrates, lower dielectric constants and edge-coupled coplanar patches yield an effective impedance bandwidth nearly ranging from 6.3 GHz to 9.5 GHz.

Applications of this antenna include battlefield communication systems, where minimal re-radiation is a necessity for safety. Furthermore, the dual-band nature of the antenna provides an ample amount of applications for communication systems such as those listed in table 2.3.1. In addition, interchangeable metamaterial lenses may be used in conjunction with this antenna design.

9. Future Work

Possible avenues to consider pursuing include the design of a complementary metamaterial lens to allow for high-gain antenna performance. These lenses are typically narrowband due to the nature of the split-ring resonators used in the lens arrays. Once a lens has been successfully simulated and fabricated, it may be redesigned for both resonant bands associated with the ARR disc antenna and ultimately use the proposed antenna as the fundamental radiating element.

Another alternative is to consider converting the present linear polarization of the antenna into an antenna that radiates circular or elliptically polarized waves. Circular polarization might be achieved through the use of a dual 90 degree offset feeds and a power divider. An ARR disc antenna that radiates a circularly polarized wave could be used in advanced communication systems or for imaging or radar applications.

Our future goal might be to design and fabricate high-gain metamaterial lenses to be used in conjunction with a metamaterial phased-array. This combination has the potential to provide improved spatial resolution in imaging and radar systems and might also be used in battlefield communication systems where radiation in directions other than the intended direction are minimized.

References

[1] Si, Li-Ming, et al. "CPW-fed compact planar UWB antenna with circular disc and spiral split ring resonators." *PIERS Proceedings, Beijing, China* (2009).

[2] Lee, Kai Fong, and Kwai Man Luk. *Microstrip patch antennas*. London: Imperial college press, 2011.

[3] Li C., Liu K. Y., Li F., "A microstrip highpass filter with complementary split ring resonators" PIERS Online, Vol. 3, pp 583-586, 2007, November 2007

[4] Yin, Xun-Cai, et al. "A compact ultra-wideband microstrip antenna with multiple notches." *Progress In Electromagnetics Research* 84 (2008): 321-332.

[5] Wang, Wentao, et al. "Dual band-notched ultra-wideband antenna with codirectional SRR." *Microwave and Optical Technology Letters* 51.4 (2009): 1032-1034.

[6] Marque, Ricardo, Martin, F., and Sorolla, Mario, "Metamaterials with Negative Parameters: Theory, Design, and Microwave Applications" John Wiley and Sons Inc Publication, 2007

[7] Brito, Davi B., et al. "Ultra wideband monopole antenna with Split Ring Resonator for notching frequencies." *Antennas and Propagation (EuCAP), 2010 Proceedings of the Fourth European Conference on*. IEEE, 2010.

[8] Hu Tao, N. I. Landy, Kebin Fan, A. C. Strikwerda, W. J. Padilla, R. D. Averitt, and Xin Zhang, "Flexible Terahertz Metamaterials: Towards a Terahertz Metamaterial Invisible Cloak" IEDM 2008 IEEE International, Dec 2008.

[9] Abul K. Azad, Hou-Tong Chen, Xinchao Lu, Jianqiang Gu, Nina R., Weisse-Bernstein, Elshan Akhadov, Antoinette J. Taylor, Weili Zhang, and John F.O'Hara, "Flexible Quasi-Three-Dimensional Terahertz Electric Metamaterials" Terahertz Science and Technology, Vol. 2, No. 1, March 2009

[10] Ahmed, Osama, and A. Sebak. "A compact UWB butterfly shaped planar monopole antenna with bandstop characteristic." *Antenna Technology and Applied Electromagnetics and the Canadian Radio Science Meeting, 2009. ANTEM/URSI 2009. 13th International Symposium on*. IEEE, 2009.

[11] Ari Sihvola, Metamaterials in electromagnetics, Metamaterials, Volume 1, Issue 1, March 2007, Pages 2-11, ISSN 1873-1988

[12] Vladimir M. Shalaev, Wenshan Cai, Uday K. Chettiar, Hsiao-Kuan Yuan, Andrey K. Sarychev, Vladimir P. Drachev, and Alexander V. Kildishev, "Negative index of refraction in optical metamaterials", Optics Letters, Vol. 30, Issue 24, pp. 3356-3358 (2005)

[13] Jason Valentine1,3, Shuang Zhang1,3, Thomas Zentgraf1,3, Erick Ulin-Avila1, Dentcho A. Genov1, Guy Bartal1 & Xiang Zhang, "Three-dimensional optical metamaterial with a negative refractive index", Nature 455, 376-379, September 2008

[14] Zhang, Y., et al. "Design and implementation of planar ultra-wideband antennas with multiple notched bands based on stepped impedance resonators." *IET microwaves, antennas & propagation* 3.7 (2009): 1051-1059.

[15] D. Schurig1, J. J. Mock, B. J. Justice, S. A. Cummer, J. B. Pendry, A. F. Starr and D. R. Smith, "Metamaterial Electromagnetic Cloak at Microwave Frquencies", Science 10 November 2006: Vol. 314 no. 5801 pp. 977-980

[16] Andrea Alù and Nader Engheta, "Multifrequency Optical Invisibility Cloak with Layered Plasmonic Shells", Phys. Rev. Lett. 100, 113901 (2008)

[17] Ricardo Marqués, Francisco Mesa, Jesús Martel, and Francisco Medina, "Comparative Analysis of Edge- and Broadside-Coupled Split Ring Resonators for Metamaterial Design – Theory and Experiments", IEEE Transactions on Antennas and Propagation, Vol. 51, No. 10, October 2003

[18] Kim, Dang-Oh, et al. "Design of the novel band notched UWB antenna with the spiral loop resonators." *PIERS Online* 6.2 (2010): 173-176.

[19] Varadan, V.V.; , "Radar Absorbing Applications of Metamaterials," Region 5 Technical Conference, 2007 IEEE , vol., no., pp.105-108, 20-22 April 2007